ELSEVIER

PII: S0142-0615(98)00011-8

Electrical Power & Energy Systems, Vol. 20, No. 7, pp. 475–487, 1998

Printed in Great Britain
0142-0615/98/$19.00+0.00

Stability analysis of induction motor networks

D H Popović[a], I A Hiskens[b] and D J Hill[a]
[a]Department of Electrical Engineering, University of Sydney, Building J13, Sydney, NSW 2006, Australia
[b]Department of Electrical and Computer Engineering, University of Newcastle, Callaghan, NSW 2305, Australia

This paper presents a stability analysis of power systems where induction motors constitute a main portion of the system load. Various stability questions are analysed in terms of network and induction motor characteristics. The issue of dynamic behaviour of induction motors under low voltage conditions is particularly addressed, highlighting the role of limits on slip variables in identifying and understanding potential (in)stability phenomena. © 1998 Elsevier Science Ltd. All rights reserved

Keywords: load system stability, induction motor loads, bifurcations

I. Introduction

The area of voltage stability analysis and control of power systems has yielded an extensive and diverse array of contributions. These are represented in several recent publications [1–3]. Motor behaviour has been a major contributing factor in a number of documented voltage instability problems and collapses [2,4]. Those incidents have typically involved large disturbances and low voltage conditions. This paper, therefore, addresses some voltage stability issues characteristic of systems where induction motor loads constitute a significant part of the system load. In particular, the focus is on sub-transmission systems, where induction motor interaction can lead to instability and stalling. With the advent of new lower voltage FACTS devices, see for example Ref. [5], an improved understanding of system dynamics at this level is very important.

The modelling of induction motor loads has been widely studied. More specifically, considerable attention has been paid to an appropriate reduced order representation of the aggregate motor dynamics in voltage stability studies [6–9]. In Refs [6,8], the first- and the higher- (third-)order induction motor models are compared in terms of their ability to capture motor load behaviour under various voltage disturbances and for the full range of motor operating conditions (from standstill to stalling). Different structural models describing the dominant dynamic behaviour of small and large induction motors are derived in Ref. [7]. A dynamic load model which describes measurable bus variables P, Q, V and frequency, and which is based on induction motor characteristics, is developed in Ref. [9].

Various voltage and system stability studies have illustrated how the choice of a load model, including induction motor load models, affects the dynamic behaviour of the system [10–19]. In Ref. [20], the voltage stability of the Rio area of the Brazilian system is assessed in terms of the proportion of the induction motor load in the total area load. In Ref. [4], several incidents in Southern California are reported. In that paper, the mechanism of voltage collapse was associated with the stalling of air-conditioning motors at low voltages and slow fault clearing. In many of these research reports, bifurcation theory is used as the main stability analysis tool [10,15,17]. Some interesting aspects of induction motor stability behaviour, based on laboratory experiments and time simulations, are presented in Refs [4,11,12,21]. In Ref. [4], tests of air conditioner response to voltage dips were used to derive a dynamic air conditioner load model appropriate for voltage stability studies.

It is now well-accepted that the voltage stability problem has both static (based on power flow equations) and dynamic (based on differential equations) aspects. Following the style of earlier results [13,14,22], the analysis of the paper addresses this systematically within a framework which emphasizes the interaction between load dynamics and the network via power balance equations. Analytical insights into observed behaviour of power systems with induction motor loads are given. The analysis makes use of bifurcation theory and time simulation. We limit attention to sub-transmission networks where the generator dynamics do not play a strong role, for example coal-mine distribution systems [23].

An interesting aspect of induction motors is that slip cannot exceed unity. These limits play an important role in system behaviour, and are carefully considered. The impact

Received 4 April 1997; accepted 4 January 1998

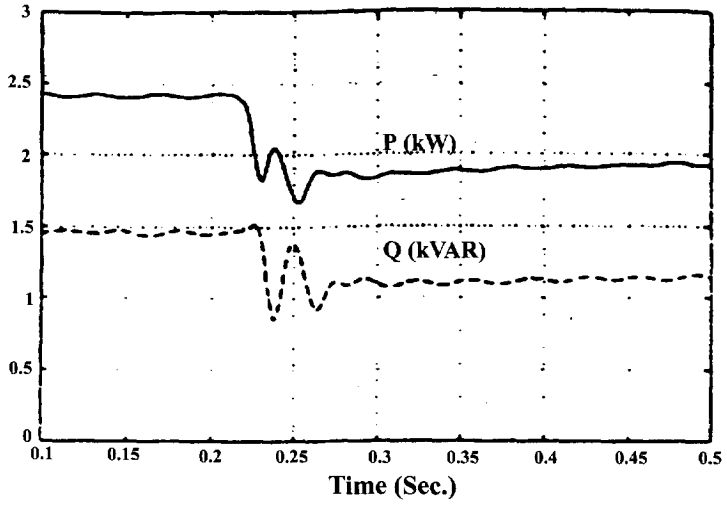

Figure 1. Experimental P and Q transients [24]

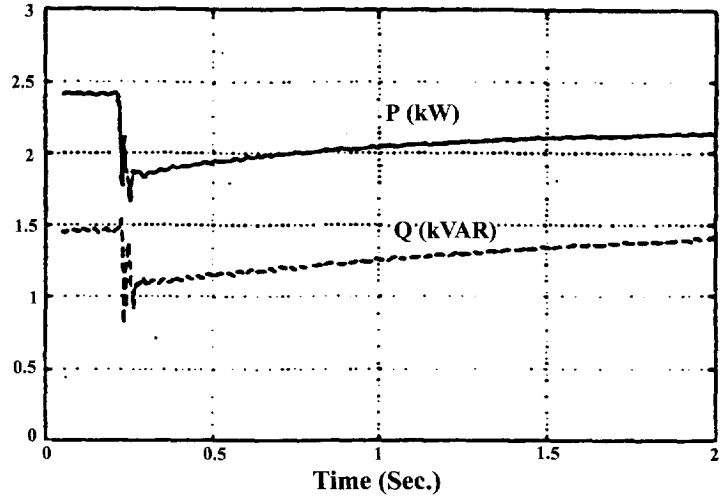

Figure 2. Experimental P and Q responses [24]

of load torque–speed characteristics and load composition on voltage and system behaviour is also addressed.

II. Load system model

II.1 *Induction motor load response*

There have been several analytical and measurement-based studies of the response of induction motors to a sudden change in voltage magnitude [11,12,24,25]. Depending on the size of the motors tested, slightly different responses have been obtained. Larger induction motors are shown in Ref. [24] to experience larger (less damped) oscillatory transients than smaller induction motors. However, regardless of the motor size, experiments show that transients disappear very quickly (within 1 s), as illustrated in Figure 1, and are followed by an almost exponential return to the steady state—see Figure 2. In the case of large induction motors though, the exponential recovery is slower [24].

Real and reactive power recovery, in response to a voltage step, is mainly determined by the motor's inertia and rotor flux time constants [26]. For long-term stability analysis, the rotor flux dynamics may sometimes be neglected [26], leaving only the first-order motor dynamics described by [18]

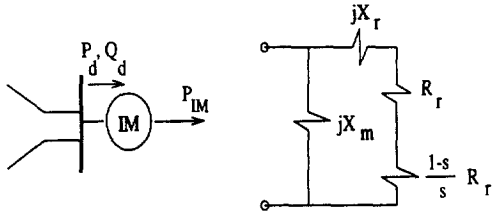

Figure 3. First-order model equivalent circuit of the induction motor

$$\dot{s} = \frac{1}{Iw_o^2}\left[\frac{P_m}{1-s} - P_{IM}(s, V)\right] \tag{1}$$

where $s = 1 - w/w_o$ is motor slip, $w_o = 2\pi f$ is synchronous speed, w is rotational speed, I is the moment of inertia, P_m is mechanical load power, and P_{IM} is the real power drawn by the induction motor. Equation (1) can be re-expressed in terms of torque variables as

$$\dot{s} = \frac{1}{Iw_o}[T_m(s) - T_e(s, V)] \tag{2}$$

where $T_e(s, V) = P_{IM}(s, V)/w_o$ is the developed electrical torque and $T_m = P_m/w$ is the load torque. This models a motor connected to a power system bus as shown in Figure 3.

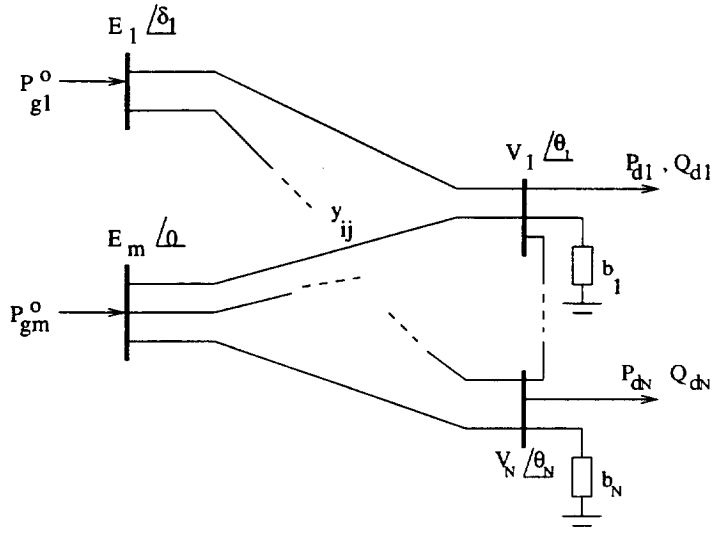

Figure 4. Load system

It is common to assume constant motor load, i.e. constant T_m. More often, however, load torque depends on the rotational speed w, with quadratic (''fan''-type load) and linear (friction effect) dependencies being the most typical torque–speed representations.

Assuming that the magnetising inductance in Figure 3 is large, i.e. $X_m \rightarrow \infty$, the real and reactive power drawn by the induction motor are given by

$$P_d = P_{IM}(s, V) = \frac{sR_r V^2}{R_r^2 + s^2 X_r^2} \tag{3}$$

$$Q_d = Q_{IM}(s, V) = \frac{s^2 X_r V^2}{R_r^2 + s^2 X_r^2} \tag{4}$$

R_r and X_r are rotor resistance and reactance respectively.

Higher-order induction motor models are shown to give more accurate stability results by being able to capture the initial oscillatory transients present in a typical motor response following a voltage step (see Figure 1). However, the essential load recovery behaviour important for longer-term system studies is captured by the first-order induction motor model. Consequently, to explore voltage collapse conditions arising from low voltages associated with large induction motor stalling, which typically occurs after the oscillations die out [17], the simplified first-order model seems to be an acceptable approximation. This is particularly so in cases where a large proportion of the system load is induction motor load [11,12,20]. The first-order model is also useful from a control point of view. By being more conservative in predicting the occurrence of stalling conditions [8], the first-order model provides control action designs, e.g. capacitor switching, that are generally also effective for the higher order model.

In Ref. [14], it was shown that the equivalent input–output representation of equations (1), (3) and (4) has the general form

$$\dot{P}_d + f_p(P_d, V) = g_p(P_d, V)\dot{V} \tag{5}$$

for the motor real power in normal (non-stalled) operation. A similar equation relates motor reactive power to voltage. As shown in Refs [14,22], the steady state described by $f_p(P_d, V) = 0$ reduces to the steady state induction motor characteristic $P_{IM}(s, V) = w_o T_m(s)$ for $s \in [0, 1]$. The transient load behaviour is obtained by integrating $g_p(\cdot)$ with respect to V. In the induction motor case, this gives equation (3) with $s = s(0)$. Hence the transient motor characteristic is proportional to the square of the voltage. When a resistor is in parallel with an induction motor, the equivalent load demand is given by

$$P_d = P_{IM}(s, V) + P_{R_o}(V) \tag{6}$$

$$Q_d = Q_{IM}(s, V) \tag{7}$$

where P_{IM} and Q_{IM} are given by equations (3) and (4) respectively, and $P_{R_o}(V) = V^2/R_o$.

II.2 *Load system model*

Consider a network of m generators (or bulk supply points), and n_b buses, as given in Refs [13,22,27]; thus there are $N = n_b - m$ buses which have no generation of real power. It is assumed that the inertia at the supply points is large relative to the loads that we are considering. Therefore, supply point loadings remain almost constant during the load disturbances of interest. Consequently, the associated dynamics are neglected, and supply points are modelled as constant real power sources of P_{gj}^o, with terminal voltages $E_j \angle \delta_j, j = 1,\ldots,m$, where the E_j are constant. This assumption is consistent with our aim of developing clearer insights into the role of load dynamics in voltage collapse disturbances such as those documented in Refs [4,23]. The $n_b - m$ load buses have voltages $V_i \angle \theta_i$, $i = 1,\ldots,n_b - m$. The angles θ_j, δ_j are referred to the phase angle of the mth generator, i.e. the n_bth bus. Line admittances are $Y_{ij} = G_{ij} + jB_{ij}$. Allowance is made for reactive power support by susceptances b_i, $i = 1,\ldots,n_b - m$. The system can be represented schematically as in Figure 4.

The $n_b - m$ loads are assumed to be induction motor loads in parallel with resistive loads. The power demand of each composite load is given by equations (6) and (7). It is assumed that the dynamics of induction motors are captured by the simplified first-order model equation (1) or equation (2), representing only mechanical dynamics.

Let P_{bi}, Q_{bi} denote the total real and reactive power leaving the ith bus via transmission lines or transformers. The standard power flow equations governing the system

network are

$$P_{di} = -P_{bi} \quad i = 1, \ldots, n_b - m \tag{8}$$

$$Q_{di} = b_i V_i^2 - Q_{bi} \quad i = 1, \ldots, n_b - m \tag{9}$$

$$P_{gj}^o = P_{bj} \quad j = n_b - m + 1, \ldots, n_b - 1 \tag{10}$$

where

$$P_{bi} := \sum_{k=1}^{n_b} V_i V_k [G_{ik} \cos(\theta_i - \theta_k) + B_{ik} \sin(\theta_i - \theta_k)],$$
$$i = 1, \ldots, n_b - 1 \tag{11}$$

$$Q_{bi} := \sum_{k=1}^{n_b} V_i V_k [G_{ik} \sin(\theta_i - \theta_k) - B_{ik} \cos(\theta_i - \theta_k)],$$
$$i = 1, \ldots, n_b - m \tag{12}$$

and for convenience we have set $V_{n_b - m + j} = E_j$ and $\theta_{n_b - m + j} = \delta_j$. As mentioned earlier, angles are referred to the n_bth bus, this bus being the slack bus. Therefore the n_bth real power equation is deleted. Note that it is a simple extension to a distributed slack formulation where all generators absorb some predetermined proportion of any power mismatch.

Following a standard procedure, we can eliminate the angles δ_j by solving the equation (10). Suppose the Jacobian matrix with elements

$$\frac{\partial P_{bj}}{\partial \delta_k}, \quad j = n_b - m + 1, \ldots, n_b - 1, \quad k = 1, \ldots, m - 1$$

is non-singular; then the Implicit Function Theorem enables us to locally express each δ_j as a function of the variables θ_i, V_i. Using equations (6) and (7), equations (8)–(10) then become in matrix form

$$P_d =: P_{IM}(s, V) + P_{R_o}(V) = P_l(\theta, V) \tag{13}$$

$$Q_d =: Q_{IM}(s, V) = Q_l(\theta, V) \tag{14}$$

where all quantities are $n_b - m$ vectors. P_l and Q_l denote $n_b - m$ vectors with components $P_{li} = -P_{bi}$ and $Q_{li} = b_i V_i^2 - Q_{bi}$ respectively.

Combining the power balance equations (13) and (14) with induction motor equations (2)–(4) gives the total system representation in the form of a differential–algebraic (DA) set of equations

$$\dot{x} = f(x, y, \mu) \tag{15}$$

$$0 = g(x, y; \mu) \tag{16}$$

where x denotes the dynamic state N-dimensional vector of induction motor slips s, y represents $2N$ power flow algebraic variables, namely bus angles θ and voltage magnitudes V (assuming no load voltages are regulated), and μ denotes a vector of parameters, e.g. E, B, P_g^o, T_m, R_r, X_r. The algebraic equations $g = 0$ define an N-dimensional manifold called the (algebraic) constraint manifold.

Note that the DA system model (equations (15) and (16)) is a state limited model since $0 \leq s \leq 1$. That is, if any of the motor loads i stall, the corresponding slip variables become fixed at $s_i = 1$. System dynamics are then driven by the remaining motor dynamics while satisfying algebraic (power balance) constraints (equation (16)). The dimension of the (algebraic) constraint manifold reduces by h, where h denotes the number of stalled motors. This $N - h$ dimensional submanifold is actually the intersection of the original constraint manifold and a new "state limit" constraint manifold of dimension h.

III. Stability analysis

We will analyse the small-disturbance system stability via the linearized version of the system model given generically by equations (15) and (16). Linearizing equations (2), (13) and (14) around the equilibrium point (s^*, y^*) gives

$$\begin{bmatrix} \Delta \dot{s} \\ 0 \end{bmatrix} = \begin{bmatrix} A_{11} & A_{12} \\ J_{sl} & J_t \end{bmatrix} \begin{bmatrix} \Delta s \\ \Delta y \end{bmatrix} \tag{17}$$

where

$$y = \begin{bmatrix} \theta \\ V \end{bmatrix}$$

$$A_{11} = \frac{1}{I w_o} \left(\frac{\partial T_m}{\partial s}(s^*) - \frac{\partial T_e}{\partial s}(s^*, y^*) \right)$$

$$A_{12} = \left[0_{N \times N} \quad -\frac{1}{I w_o} \frac{\partial T_e}{\partial V}(s^*, y^*) \right]$$

$$J_t(s, \theta, V) = \begin{bmatrix} -\frac{\partial P_l}{\partial \theta} & \frac{\partial P_d}{\partial V} - \frac{\partial P_l}{\partial V} \\ -\frac{\partial Q_l}{\partial \theta} & \frac{\partial Q_d}{\partial V} - \frac{\partial Q_l}{\partial V} \end{bmatrix}$$

$$J_{sl}(s, V) = \begin{bmatrix} \frac{\partial P_d}{\partial s} \\ \frac{\partial Q_d}{\partial s} \end{bmatrix}$$

It is clear that J_t is dependent upon the network and the transient load characteristics P_d, Q_d described by equations (6) and (7).

Eliminating the algebraic variables y, assuming J_t is non-singular, gives

$$\Delta \dot{s} = (A_{11} - A_{12} J_t^{-1} J_{sl}) \Delta s = A \Delta s \tag{18}$$

These dynamics are well-defined away from the singular surface $\det J_t = 0$. If the system (18) is stable and equilibria do not lie on the singular surface, then the original DA system is stable [28].

Result 1. Assume $\det J_t(s^*, y^*) \neq 0$. The load system of equations (2), (13) and (14) at operating point (s^*, y^*) is small disturbance stable iff the matrix $(A_{11} - A_{12} J_t^{-1} J_{sl})$ with all matrices evaluated at (s^*, y^*), is (asymptotically) stable.

This result establishes asymptotic stability properties of an equilibrium point, i.e. whether the real parts of all the eigenvalues of A are negative. As several voltage stability studies have indicated, the appearance of a zero (real) eigenvalue (saddle-node bifurcation) or an imaginary axis crossing of a complex conjugate pair (Hopf bifurcation), may be used as an indicator of the proximity to instability (voltage collapse) problems—see Refs [1,13,15,17,22,29,30] and references cited therein. Eigenvalue analysis can be used to evaluate the effects of varying some system parameter on voltage stability. Time simulations may be used to verify the eigenvalue-based predictions and to give the complete dynamic response.

IV. Single load example

In order to explore in more detail the role of induction motor loads in voltage stability studies the power system shown in Figure 5 is considered. The motor data are adapted from Ref. [23]. This system represents a typical supply scheme where a generator feeds a composite load through a transmission and/or distribution system impedance. Many stability aspects of this single induction motor load example are known, but it is useful to revisit them in the above analytical framework and clarify associated bifurcation behaviour. The analysis focuses on stability and control issues encountered during system operation under heavy load conditions; the impacts of load torque–speed characteristics, motor parameters and load composition are studied. Special consideration is given to system behaviour under low voltage conditions. The possibility of preventing voltage collapse by capacitor switching, as mentioned in Refs [3,18,31], will also be demonstrated.

IV.1 *Load torque–speed characteristic*

The influence of load torque–speed characteristics on the behaviour of the system of Figure 5 is studied by employing eigenvalue and bifurcation analysis. By expressing the load torque as $T_m = (k/w_o)w^a$, the parameter k can be used as a bifurcation parameter to study the changes in equilibria which result from changes in the load torque, i.e. the load power demand. Three particular load torque–speed characteristics are considered: constant torque ($a = 0$), torque proportional to speed ($a = 1$) and torque proportional to the square of speed ($a = 2$).

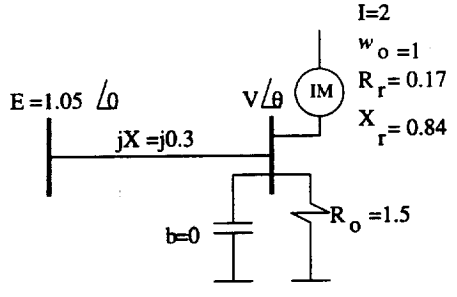

Figure 5. Single composite load system

IV.1.1 *Case 1: constant torque motor operation*

In the case of constant torque motor operation, with $T_m = k/w_o$ as the bifurcation parameter, the motor demand–voltage curve becomes the bifurcation diagram. (Recall that in per unit, at steady state $P_{IM} = T_e = T_m$.) This is illustrated in Figure 6 by the dashed lines. The P_{IM}–V curve shows the projection of $P_{IM}(s, V)$ in the P–V plane, whereas the P_{IM}–s curve shows the projection in the P–s plane. The system loses stability at the saddle-node bifurcation point which corresponds to the turning points of the P_{IM}–V and P_{IM}–s curves.

However, the saddle-node point lies on the lower part of the total load demand–voltage (P_d–V) curve shown in Figure 6 as a solid line. (The total load demand includes the resistive load.) Note that the saddle-node point does not coincide with the maximum total power loadability. This is because the curve shows the total load power, whereas the bifurcation parameter is the motor torque (or, equivalently, motor demand). The position of the saddle-node point depends on the proportion of the total load demand which is resistive (68% in this case). As a result, it is possible for the system to maintain stable operation even on the lower part of the P_d–V curve. Note though that as soon as the load torque becomes greater than the critical (saddle-node) torque value $T_{cr} = 0.4463$ pu, given by the turning point of the dashed curves in Figure 6, the motor starts stalling, i.e. motor speed decreases. Referring to equation (2), in such operating conditions the difference between the electrical torque and the load torque results in a sustained slip increase. This, in turn, causes a voltage decrease accompanied by an increase in the absorbed motor reactive power and further voltage degradation. Such a stalling situation, arising from the sudden increase of the load torque to $T_m = 0.55$ pu, is depicted in Figure 7.

By increasing the proportion of the induction motor load in the total load power demand, the saddle-node bifurcation point moves closer to the maximum loadability point. The stalling conditions occur at a higher speed, therefore representing a more critical situation. Alternatively, by increasing the resistive part of the load (whilst keeping the total nominal load constant), stalling conditions will occur at a lower speed and voltage. This is in an agreement with the measured results presented in Ref. [21].

With the same system and motor data, but with the load torque as a linear or quadratic function of speed, different situations may arise. These cases will now be considered.

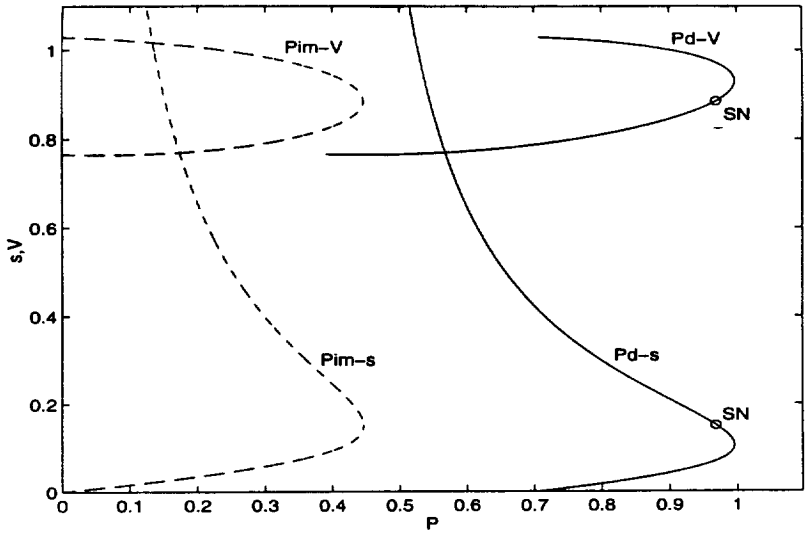

Figure 6. Bifurcation diagram: constant torque motor operation

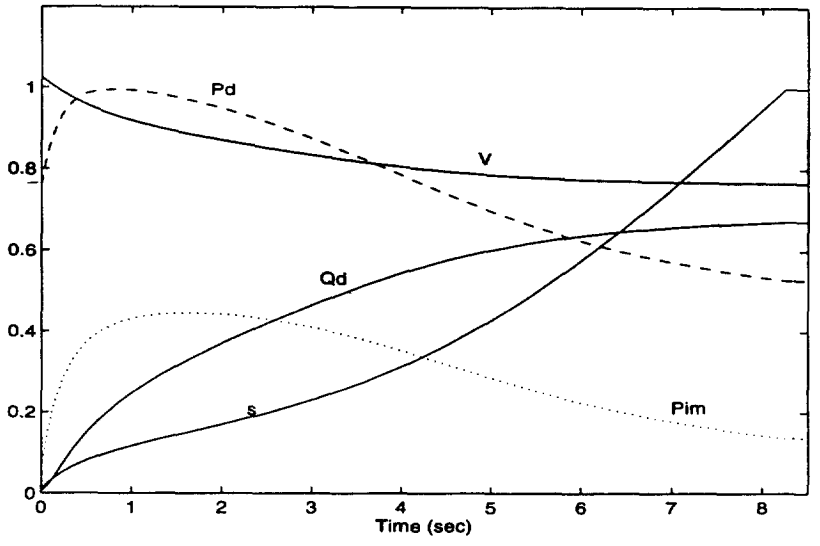

Figure 7. Time simulation of the stalling conditions; $T_m = 0.55$ pu

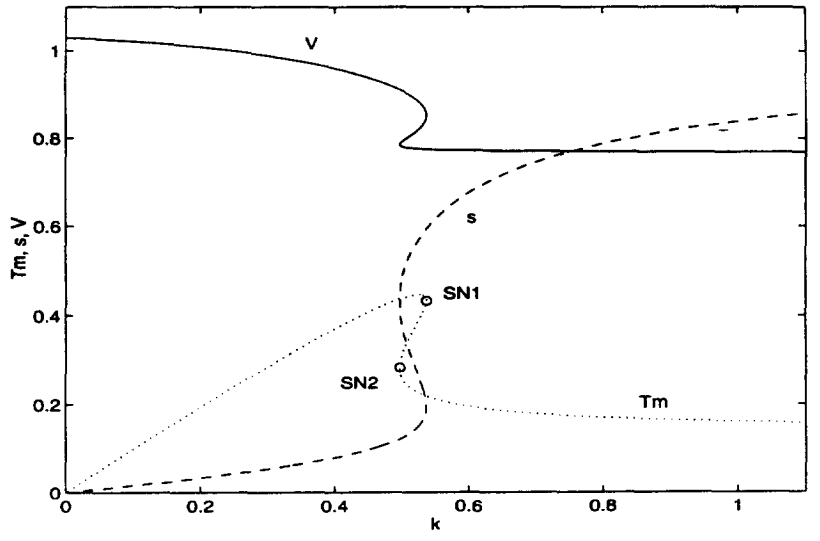

Figure 8. Bifurcation diagram: linear torque–speed characteristic

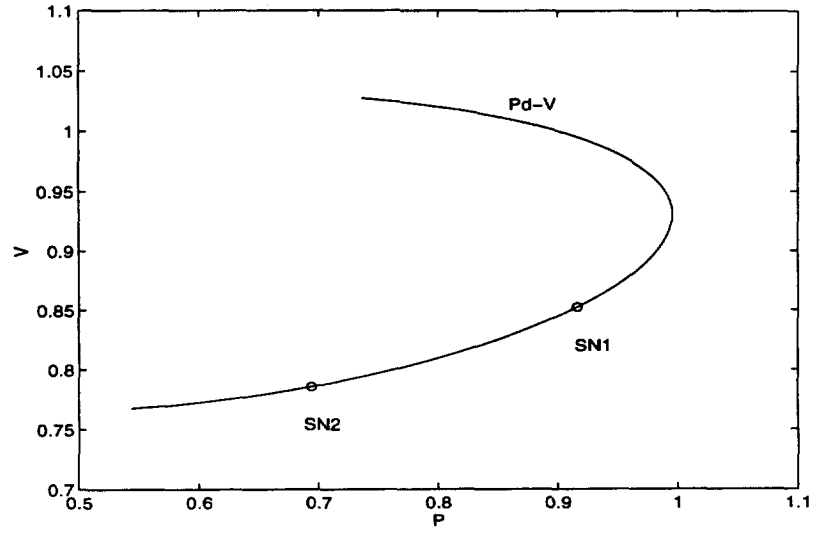

Figure 9. P_d–V curve for the linear torque–speed characteristic

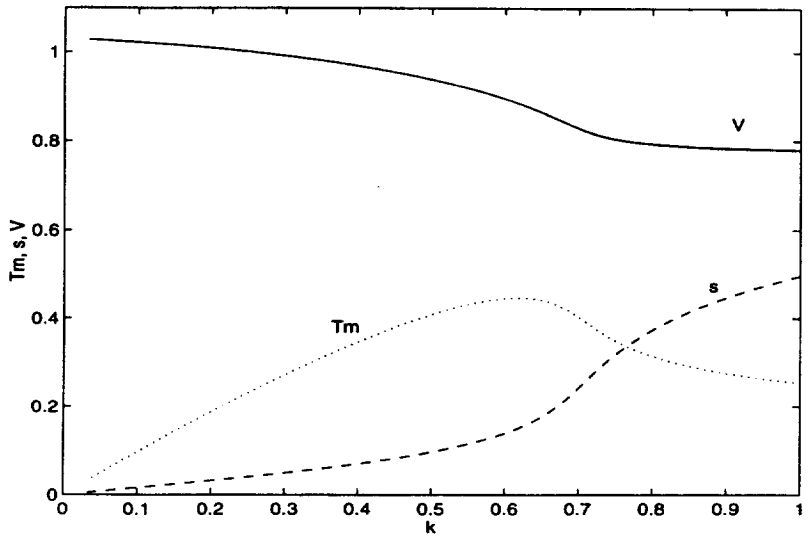

Figure 10. Bifurcation diagram: quadratic torque–speed characteristic

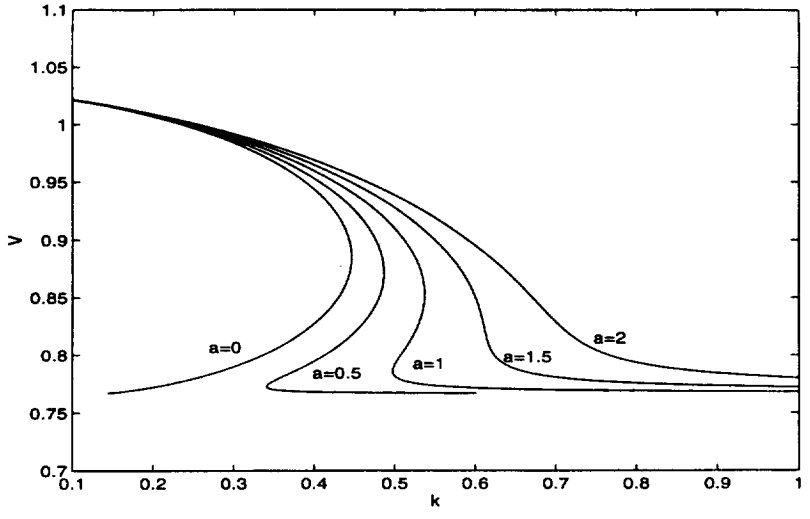

Figure 11. Bifurcation diagrams for various load torque–speed characteristics

IV.1.2 Case 2: load torque as a linear function of speed

Figure 8 illustrates the bifurcation diagram, as seen from different projections, when a linear torque–speed dependence (i.e. $a = 1$) is modelled. It is easy to see that in a range of the load parameter k between the saddle-node points SN1 and SN2, there are three equilibrium points. Stable points occur on the low slip–high voltage and the higher slip–lower voltage branches of the bifurcation curve. An unstable point lies on the part of the bifurcation curve between the two saddle-node bifurcation points. By replotting the bifurcation diagram in the P–V plane as shown in Figure 9, it can be seen that both saddle-node bifurcation points lie on the lower part of the P_d–V curve. Referring to Figure 8, it is interesting to note that for every load torque coefficient k, there is at least one stable equilibrium point. Since the unstable equilibrium point regains stability through the bifurcation point SN2, stable operating conditions can be maintained even when motor speed significantly decreases. As shown in Figure 8, the corresponding voltage level may still not be so critically low as to indicate voltage collapse.

Even though the operating situation with higher slip is generally not desirable, some motors (for example traction motors in mines) are designed to function at higher slip values [23].

IV.1.3 Case 3: load torque as a quadratic function of speed

The situation is even less critical when the load torque is a quadratic function of speed (i.e. $a = 2$). Figure 10 illustrates that for this example, a single stable equilibrium point exists for all values of the load parameter k. Whilst the P_d–V and P_d–s curves retain the same (''nose'' type) shape as in the cases of linear and constant load torque–speed characteristics in Figures 6, and 9, the bifurcation diagram (Figure 10) differs and does not indicate the existence of any bifurcation points. Consequently, unstable equilibria do not arise in this particular example power system. The analysis also shows that for the chosen system data, the load composition does not influence system behaviour, i.e. the system is small disturbance stable irrespective of the proportion of the induction motor load in the total load.

The three cases have clearly illustrated that system stability is highly dependent on load torque–speed

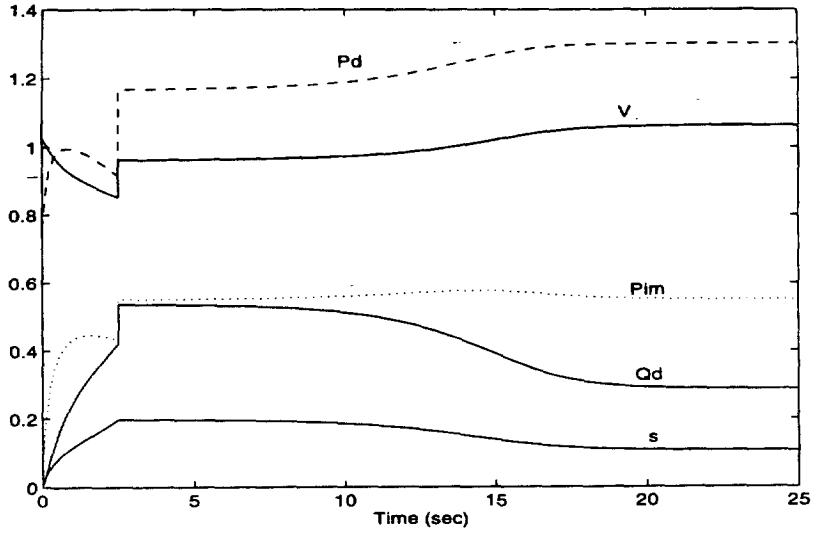

Figure 12. Time simulation of the capacitor switching at $t = 2.5$ s

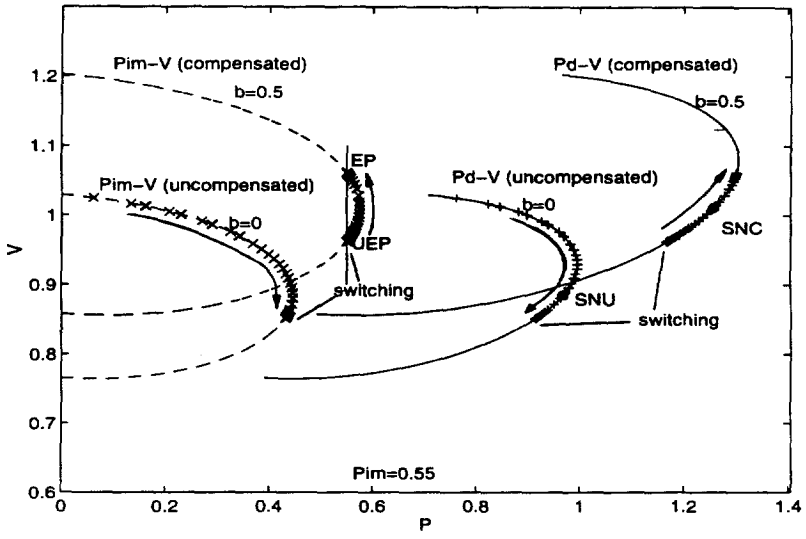

Figure 13. Capacitor switching at $t = 2.5$ s as seen in the P–V plane

characteristics. More specifically, the analysis has indicated that the load torque–speed index a is a critical parameter which can significantly affect the stability properties of the system. These effects are closely linked with the shape of the bifurcation diagram and the bifurcations which can occur under load variation. Figure 11 gives a closer insight into the effect of the load torque–speed index a on bifurcations and stability. As a increases, the number of saddle-node bifurcations, corresponding to the turning points of the bifurcation curves, changes from 1 (for $a = 0$) to 2 (for $0 < a \approx 1.35$). For $a \approx 1.35$, there are no saddle-node bifurcations. These bifurcations in parameter a depend of course on the system parameters; for example, it has been found that a quadratic torque–speed characteristic associated with a motor that has slightly different R_r and X_r parameters (e.g. $R_r = 0.01$, $X_r = 0.05$) may lead to a situation similar to that shown in Figure 8.

IV.1.4 Summary

The most vulnerable situation occurs when the motor operates under constant load torque. The saddle-node bifurcation point occurs at a higher voltage level and at higher speed than when the load torque is speed dependent. Also, in the case of $T_m = const$, values of load torque above the bifurcation value imply motor stalling and eventual voltage collapse—see Figure 7. However, such unstable behaviour may be alleviated if the load torque is dependent on speed. Moreover, as Figures 10 and 11 (for $a \approx 1.35$) indicate, the load system may remain stable even though the motor operates at an unacceptably low speed. The possibility for multiple stable operating points is shown to exist.

It is also worth pointing out that for the chosen system data and motor characteristic, the percentage of induction motor load in the total load demand does not affect the nature of bifurcations, only the parameter values at which the bifurcations occur.

IV.2 *Prevention of voltage collapse by capacitor switching*

Motor stalling, as illustrated in Figure 7, can be avoided by capacitor switching [3,18,31]. This is shown in Figure 12. The capacitor-compensated network is able to deliver a higher electrical torque. As a result, the saddle-node point for the compensated system (point SNC in Figure 13) occurs at a higher load power. The control action shown in Figure 12 is successful, even though, just before the capacitor is switched, the system trajectory is well on the lower part of

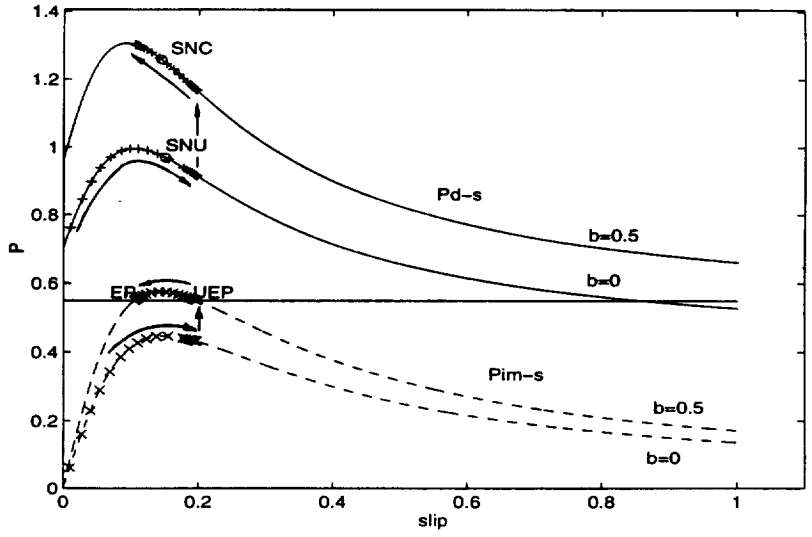

Figure 14. Capacitor switching at $t = 2.5$ s as seen in the P–s plane

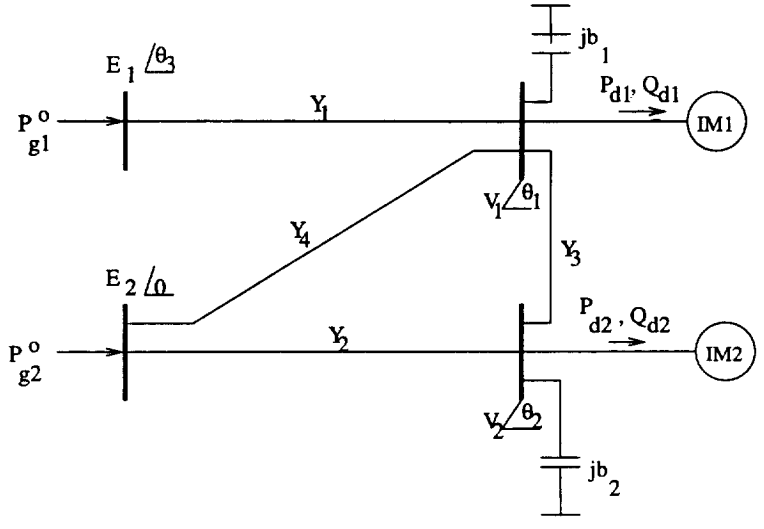

Figure 15. Model system

Table 1. Model parameters

E_1	E_2	P_{g1}^o	b_1	b_2	Y_i	I_1	I_2	w_{oi}	R_{r1}	R_{r2}	X_{ri}
1.3	1	0.1736	0.15	0.1	$-j1$	2	1.8	1	0.17	0.15	0.2

the (uncompensated) P_d–V curve and below the saddle-node point SNU. The capacitor switching time is chosen so that the value of slip at the time of switching is smaller than the value of slip at the unstable compensated equilibrium point (point UEP in Figure 14). This switching strategy ensures that, after switching, the system trajectory moves towards the stable compensated equilibrium point (point EP in Figure 14) and stops when that point is encountered.

This control criterion is equivalent to the minimum voltage criterion proposed in Ref. [31]. The minimum voltage criterion requires that, after the insertion of reactive support, the immediate operating voltage must be higher than a minimum voltage determined by the intersection of the steady state load characteristic and the final network curve. In the induction motor case, the minimum voltage point corresponds to the lower point of intersection of the vertical line drawn at $P_{IM} = w_o T_m = 0.55$ pu and the compensated bifurcation diagram, i.e. the compensated P_{IM}–V curve. This is shown as point UEP in Figure 13. The capacitor switching results in an immediate positive mismatch between the electrical supply and the mechanical demand which eventually preserves the system stability.

V. Multi-load example

The analysis of a multi-induction motor case reveals the possibility of more diverse power system behaviour than in the above simple example. The system of Figure 4 with $m = N = 2$, as shown in detail in Figure 15, is considered. The system loads are purely induction motor loads, i.e. there are no resistive loads. We shall assume $T_{mi} = const$, $i = 1,2$. The system data are given in Table 1. Note that the same system

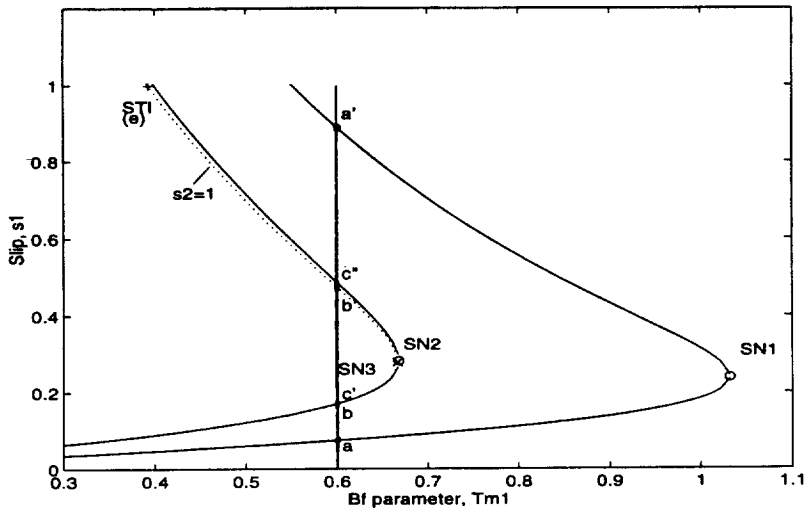

Figure 16. Bifurcation diagram in the T_{m1}–s_1 plane

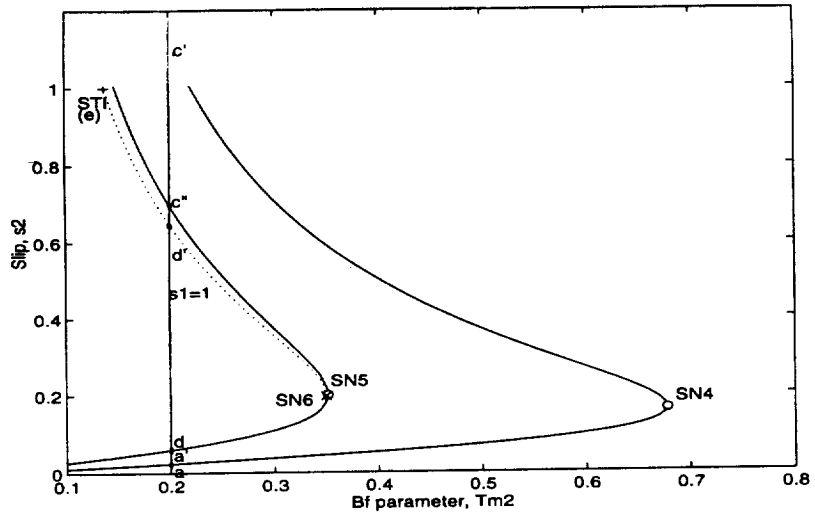

Figure 17. Bifurcation diagram in the T_{m2}–s_2 plane

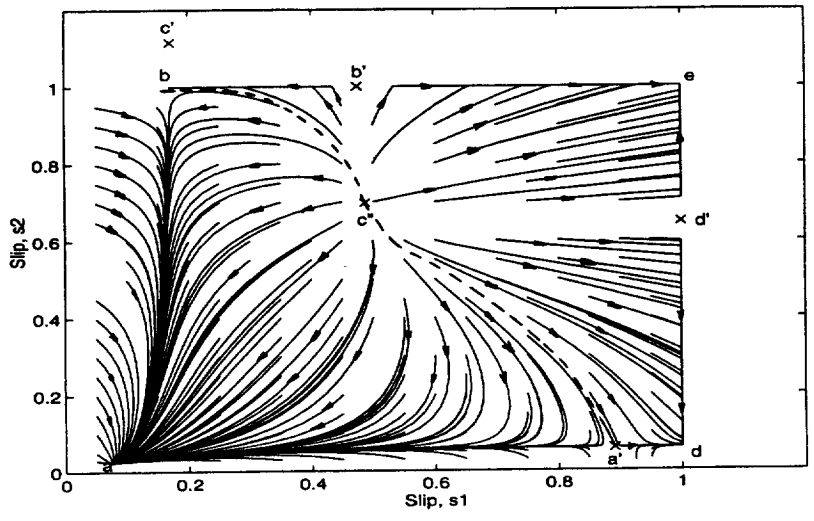

Figure 18. Slip trajectories

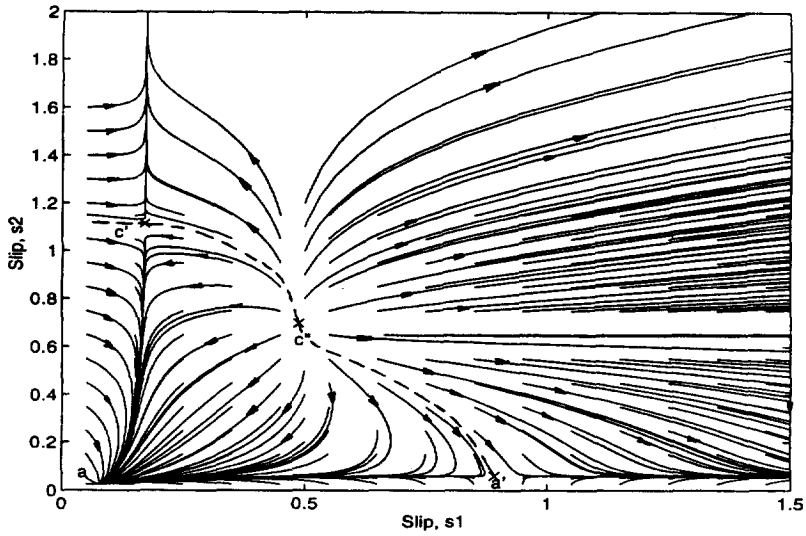

Figure 19. Slip trajectories without slip limits

and its constraints were considered in Refs [13,22], except that there the reactive power loads were of the generic recovery type [14].

V.1 *Bifurcation points*

Figure 16 illustrates the bifurcation diagram with the load torque T_{m1} as the bifurcation parameter. The two solid lines represent bifurcation branches which correspond to normal motor operation (meaning no stalled motors) with the load torque $T_{m2} = 0.2$ pu. The dotted line denotes a bifurcation branch along which $s_2 = 1$, i.e. induction motor IM2 is stalled. (In this projection, the lines are very close together, but along the dotted line $s_2 = 1$.) A similar bifurcation diagram with the load torque T_{m2} as the bifurcation parameter is presented in the T_{m2}–s_2 plane in Figure 17. Solid lines again represent bifurcation branches which correspond to normal operation of the motors when the load torque $T_{m1} = 0.6$ pu. The dotted line represents the bifurcation branch composed of equilibrium points with IM1 stalled.

Four bifurcation points are denoted in Figure 16: SN1, SN2 and SN3 are saddle-node bifurcation points, whilst STI will be called a stalling-induced bifurcation point. That point is a special limit-induced bifurcation point [32] which corresponds to a solution of the algebraic equations (equation (16)) with $s_1 = 1$, $s_2 = 1$. That is, the system representation loses its dynamic nature at that point but the number of potential equilibrium points changes by one when the load torque values exceed the values corresponding to the STI point. Note that the nature of bifurcation points SN1 and SN2 is different to that of SN3; points SN1 and SN2 arise with normal operation of both motors under variation of the load torque T_{m1}, whilst point SN3 arises under T_{m1} variation but with state variable s_2 being on its limit. With the state s_2 limit being active, the new bifurcation point (point STI) emerges when the other state variable s_1 encounters its limit. Additionally, three saddle-node points (points SN4, SN5 and SN6 in Figure 17) exist corresponding to the load torque T_{m2} being the bifurcation parameter. The occurrence of a total of seven bifurcation points, including the three stalling-related bifurcation points SN3, SN6 and STI, has interesting implications for the system behaviour. This can be explored through an analysis of the equilibrium points and their stability.

As mentioned in Section III, the stability of the system equilibria can be predicted by the eigenstructure of the system matrix A. Note, however, that the reduced order system dynamic representation should be used when assessing the small disturbance stability of the stalling-related equilibria, i.e. the equilibria with $s_1 = 1$ or $s_2 = 1$. More specifically, in the case of IM2 stalled, only the dynamics of the unstalled motor IM1 should be represented in the system model (equations (15) and (16)). Similarly, when s_1 is on its limit the system representation should capture only the remaining free dynamics, i.e. the dynamics of the motor IM2. The occurrence of the saddle-node bifurcation points SN3 and SN6 is associated with the appearance of a zero eigenvalue in the state matrix of the appropriately reduced system model.

The analysis of the eigenvalues of system equilibria depicted in Figures 16 and 17 shows that saddle-node points SN1, SN3, SN4, SN6 separate stable equilibria on the lower half branches from unstable equilibria on the upper side of the bifurcation branches. This indicates the possibility of multiple stable operating points. On the other hand, saddle-node points SN2 and SN5 separate unstable equilibria (saddles) on the lower half branches from unstable equilibria (sources) on the upper side of the bifurcation branches.

V.2 *Dynamical behaviour*

We now consider how this diverse bifurcation structure has a significant impact on the behaviour of system trajectories. Figure 18 illustrates a case with load torque values set to $T_{m1} = 0.6$ pu and $T_{m2} = 0.2$ pu. As predicted by the bifurcation diagrams of Figures 16 and 17, four of the potential nine equilibria are dynamically stable. The operating point a is the normal operating point. No slip variables are on limits at that point. Operating points b, d and e are stable limit-induced operating points. The normal unstable equilibrium points are denoted by a′, c′ and c″, whilst points b′ and d′ are limit-induced unstable equilibria. It is interesting to note the influence of point c″ on the overall behaviour of trajectories. Since point c″ is an unstable node, it acts as a source with all trajectories directed away from it. However, the trajectories stop when any of the operating points a, b, d or e are encountered. Note though that points b, d and e are stable only because one or both state variables, i.e. slips, hit their limits and become constant, leaving reduced or no

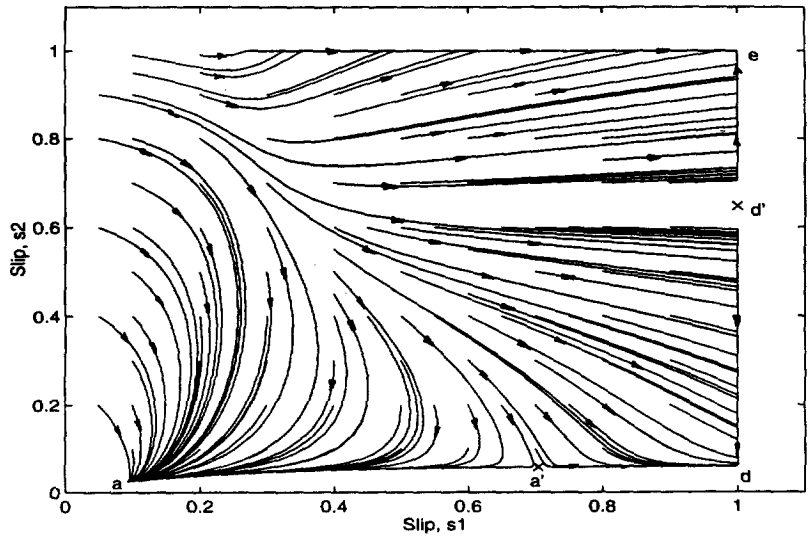

Figure 20. Slip trajectories for $T_{m1} = 0.7$ pu, $T_{m2} = 0.2$ pu

dynamics to govern system behaviour. To gain a better insight into the effect of slip limits on system stability, the phase portrait for the same case but without limits is shown in Figure 19. The trajectories which leave the source point stop only when the operating point a is reached. All other equilibria in this artificial case are unstable. Note that, in this case, the bifurcation diagrams of Figures 16 and 17 reduce to only two bifurcation branches denoted by the solid lines in Figures 16 and 17.

The stability boundary of the (normal) operating point a is shown as a dashed line in Figures 18 and 19. It is clear that the limit on slip s_2 causes an appreciable change in the shape of the boundary in the region of point b. (Note that the algebraic Jacobian $D_y g$ is globally non-singular in both cases, since the load is transiently a conductance [33].) The appearance of limit-induced equilibria explains the slightly smaller region of attraction of the operating point a in the slip-limited case. More specifically, since the trajectories which hit the limit $s_2 = 1$ do not come off that boundary, the region of attraction of the operating point a near point b is slightly smaller in the case of Figure 18.

Point c′ with $s_2 > 1$ (braking operating mode) has a strong influence on the structure of the flows in the restricted state space. Figures 18 and 19 clearly show that the unstable manifold of point c′ which runs to point a is a dominant feature.

Figure 18 allows a useful interpretation of limit-induced equilibrium points b, b′, d, d′. Each of those equilibria correspond to points where trajectories are normal to the limit surface. At those points, the component of movement of the non-restricted slip state along the limit surface, i.e. the surface where the other slip state is fixed at unity, is zero. Hence the system is in equilibrium at those points. The stability of the equilibria is determined by the component of movement of the non-restricted slip state near the equilibria. As mentioned earlier, mathematically this is the same as finding the eigenvalues of the "reduced" Jacobian, i.e. the Jacobian of the system taking into account the algebraic limit constraints. These issues are explored further in Refs [32,34].

It is useful to note another aspect of identifying the bifurcation points under slip-limited conditions, i.e. points SN3 and SN6. Based on load torque values at these critical points, the changes in system limit-induced operating points under changing loading conditions can be predicted. Figure 18 illustrates the case with four stable operating points. Assuming an increase in the load torque values T_{m1} and/or T_{m2}, some of the limit-induced operating points may lose stability and/or disappear at limit-induced bifurcation points SN3 and SN6. A sustained load torque increase would lead eventually to only one remaining operating point, where both induction motors were stalled. Referring to Figures 16 and 17, note that such a situation would be accompanied by the disappearance of the source, i.e. the unstable equilibrium point c″. Figure 20 illustrates the case when the load torque T_{m1} is increased to $T_{m1} = 0.7$ pu. Since T_{m1} now exceeds the values corresponding to bifurcations SN2 and SN3, (see Figure 16), the equilibrium points c″, c′, b and b′ disappear. The loss of point b means that, when compared with the case $T_{m1} = 0.6$ pu in Figure 18, the total number of stable operating points has reduced by one. Also, it is worth noting that the region of attraction of the normal operating point a has become smaller, whilst the stability regions of stalling-induced equilibria d and e have been significantly extended.

This multi-load case has clearly pointed out the importance of slip limits and their significant effect on the stability and behaviour of motor load systems. The existence of multiple operating points, induced by the stalling of different motors, is an inherent feature of power systems with induction motor loads. Note that even though points b, d and e are theoretically stable, operation under stalled conditions would generally not be allowed. The stalled motors would trip off-line. The voltage viability problem associated with these conditions can be adequately treated by the use of appropriately fast capacitor switching, as discussed in Section IV.2.

VI. Conclusions

This paper presents a systematic analysis of the dynamical behaviour and stability of power systems which contain a large percentage of induction motor loads. The dynamic behaviour of induction motors under changing loading conditions has been analytically characterized based on the analysis of system bifurcations. The load torque–speed characteristic is shown to have a significant influence on system stability, especially under low voltage conditions.

In multi-load systems, a rich set of non-linear phenomena is directly linked to the presence of state limits, i.e. limits on motor slip variables. These limits lead to multiple stable operating points and multiple stability regions which do not exist in the unlimited state system model. The stability boundary is shown to be strongly affected by stalling-induced equilibria. The slip limits generate some new bifurcations which determine critical parameter values at which qualitative changes in system behaviour occur. In particular, we identify a new concept of stalling-induced bifurcations related to the operating conditions with all induction motors being stalled. The appropriate system modelling when stalling conditions arise, i.e. when slip limits become active, is shown to be necessary in order to identify analytically the various stability features of power systems with induction motor loads. It allows the possibility of fully understanding diverse dynamic behaviour of induction motors and the associated instability mechanisms in power systems.

The analytical approach presented in this paper complements the traditional measurement and time-domain simulation approaches. It also provides an important mathematical foundation for control design. Current work in the development of global control schemes able to cope with various operating conditions and associated complex behaviour is directly applicable to induction motor networks. These control topics are beyond the scope of this paper and will be reported elsewhere.

VII. References

1. Concordia, C. (ed.), Special issue on voltage stability and collapse. *International Journal of Electrical Power and Energy Systems*, 1993, **15**(4).
2. Mansour, Y. (ed.), *Voltage Stability of Power Systems: Concepts, Analytical Tools and Industry Experience*. IEEE Task Force Report, Publication 90TH 0358-2-PWR, 1990.
3. Taylor, C. W., *Power System Voltage Stability*. McGraw-Hill, 1994.
4. Williams, B. R., Schmus, W. R. and Dawson, D. C., Transmission voltage recovery delayed by stalled air conditioner compressors. *IEEE Transaction on Power Systems*, 1992, **7**(3), 1173–1179.
5. Grönqvist, J., Andersson, G. and Ekström, Å., Current limiting devices: a new concept for improving power quality. *Proceedings of APSCOM'97*, Hong Kong, 1997.
6. Ahmed-Zaid, S., Taleb, M. and Price, W. W., First-order induction machine models near voltage collapse. In *Proceedings of NSF/ECC Workshop on Bulk Power System Voltage Phenomena—II: Voltage Stability and Security*, Deep Creek Lake, MD, 1991.
7. Ahmed-Zaid, S. and Taleb, M., Structural modelling of small and large induction machines using integral manifolds. *IEEE Transactions on Energy Conversion*, 1991, **6**(3), 529–535.
8. Jimma, K., Tomac, A., Vu, K. and Liu, C.-C., A study of dynamic load models for voltage collapse analysis. In *Proceedings of NSF/ECC Workshop on Bulk Power System Voltage Phenomena—II: Voltage Stability and Security*, Deep Creek Lake, MD, 1991.
9. Lesieutre, B. C., Sauer, P. W. and Pai, M. A., Development and comparative study of induction machine based *P,Q* load model. *IEEE Transactions on Power Systems*, 1995, **10**(1), 182–191.
10. Alvarado, F. L., Voltage stability including detailed load models. In *Proceedings of NSF/ECC Workshop on Bulk Power System Voltage Phenomena—III: Voltage Stability, Security and Control*, Davos, Switzerland, 1994.
11. Borghetti, A. *et al.*, On dynamic load models for voltage stability studies. IEEE/PES Winter Meeting Paper No 96WM 281-6 PWRS, Baltimore, 1996.
12. Gustafsson, M., Krantz, N. and Daalder, J., Voltage stability: the significance of induction motor loads. In *Proceedings of the 27th Annual North American Power Symposium*, Bozeman, MT, 1995, pp. 394–402.
13. Hill, D. J., Hiskens, I. A. and Popović, D. H., Stability analysis of power system loads with recovery dynamics. *International Journal of Electrical Power and Energy Systems*, 1994, **16**(4).
14. Hill, D. J., Nonlinear dynamic load models with recovery for voltage stability studies. *IEEE Transactions on Power Systems*, 1993, **8**(1), 166–176.
15. Overbye, T. J., Effects of load modelling on analysis of power system voltage stability. *International Journal of Electrical Power and Energy Systems*, 1994, **16**(5), 329–338.
16. Pal, M. K., Voltage stability conditions considering load characteristics. *IEEE Transactions on Power Systems*, 1992, **7**(1), 243–249.
17. Sauer, P. W. and Lesieutre, B. C., Power system load modelling. In *Systems and Control Theory for Power Systems*, ed. J. H. Chow, P. V. Kokotovic and R. J. Thomas. Springer, 1995, pp. 283–315.
18. Sekine, Y. and Ohtsuki, H., Cascaded voltage collapse. *IEEE Transactions on Power Systems*, 1990, **5**(1).
19. Thomas, R. J. and Tiranuchit, A., Dynamic voltage instability. In *Proceedings of the 26th Conference on Decision and Control*, Los Angeles, CA, 1987.
20. Pinto, H. J. C. P. *et al.*, Modal analysis for voltage stability—application at base case and point of collapse. In *Proceedings of NSF/ECC Workshop on Bulk Power System Voltage Phenomena—III: Voltage Stability, Security and Control*, Davos, Switzerland, 1994, pp. 215–228.
21. Krantz, N., Gustafsson, M. and Daalder, J., Voltage collapse with a laboratory power system model. In *Proceedings of the IEEE/KTH Stockholm Power Technology Conference*, Stockholm, Sweden, 1995, pp. 191–196.
22. Hill, D. J., Hiskens, I. A. and Popović, D. H., Load recovery in voltage stability analysis and control. In *Proceedings of NSF/ECC Workshop on Bulk Power System Voltage Phenomena—III: Voltage Stability, Security and Control*, Davos, Switzerland, 1994.
23. Waudby, J. F., Voltage stability indicators for underground coal mine electrical systems. Undergraduate thesis, University of Newcastle, Australia, 1992.
24. Lem, T. Y. J. and Alden, R. T. H., Comparison of experimental and aggregate induction motor responses. *IEEE Transactions on Power Systems*, 1994, **9**(4), 1895–1900.
25. Taleb, M., Akbab, M. and Abdullah, E. A., Aggregation of induction machines for power system dynamic studies. *IEEE Transactions on Power Systems*, 1994, **9**(4), 2042–2048.
26. Task Force on Load Representation for Dynamic Performance, Load representation for dynamic performance analysis. *IEEE Transactions on Power Systems*, 1993, **8**(2), 472–482.
27. Abe, S. and Isono, A., Determination of power system voltage stability, part 1: theory. *Electrical Engineering in Japan*, 1976, **96**(2), 70–77.
28. Hill, D. J. and Mareels, I. M. Y., Stability theory for differential/algebraic systems with application to power systems. *IEEE Transactions on Circuits and Systems*, 1990, **37**(11), 1416–1423.
29. Kundur, P., *Power System Stability and Control*. McGraw-Hill, 1994.
30. Kwatny, H. G., Pasrija, A. K. and Bahar, L. Y., Static bifurcations in electric power networks: loss of steady-state stability and voltage collapse. *IEEE Transactions on Circuits and Systems*, 1986, **33**(10), 981–991.
31. Xu, W., Mansour, Y. and Harrington, P. G., Planning methodologies for voltage stability limited power systems. *International Journal of Electrical Power and Energy Systems*, 1993, **15**(4).
32. Venkatasubramanian, V., Jiang, X., Schättler, H. and Zaborszky, J., Current status of the taxonomy theory of large power system dynamics—DAE systems with hard limits. In *Proceedings of NSF/ECC Workshop on Bulk Power System Voltage Phenomena—III: Voltage Stability, Security and Control*, Davos, Switzerland, 1994, pp. 15–103.
33. Hiskens, I. A. and Hill, D. J., Modelling of dynamic load behaviour. In *Proceedings of NSF/ECC Workshop on Bulk Power System Voltage Phenomena—III: Voltage Stability, Security and Control*, Davos, Switzerland, 1994.
34. Praprost, K. L. and Loparo, K. A., A stability theory for constrained dynamic systems with applications to electric power systems. *IEEE Transactions on Automatic Control*, 1996, **41**(11), 1605–1617.